Activation Persulfate by Various Iron-Based Catalysts

Subjects: Chemistry, Applied

Contributor: Keke Zhi

Advanced oxidation technology of persulfate is a new method to degrade wastewater. As the economy progresses and technology develops, increasingly more pollutants produced by the paper industry, printing and dyeing, and the chemical industry are discharged into water, causing irreversible damage to water. Methods and research directions of activation persulfate for wastewater degradation by a variety of iron-based catalysts are reviewed. This entry describes the merits and demerits of advanced oxidation techniques for activated persulfate by iron-based catalysts. In order to promote the development of related research work, the problems existing in the current application are analyzed.

Keywords: iron-based catalysts ; activation persulfate ; degrading wastewater

1. $MeFe_2O_4$ (Me = Cu, Co, Zn, etc.)

In terms of activation mechanism, transition metal compounds react with PS to produce a large amount of $\cdot SO_4^-$; the reaction equation follows:

$$M^{n+} + S_2O_8^{2-} \rightarrow M^{(n+1)+} + \cdot SO_4^- + SO_4^{2-}$$

(1)

As can be seen from the above reaction, metal ions are in a free state dispersed in the solution during the reaction process. Although the wastewater can be degraded by the activation persulfate mechanism, it belongs to homogeneous catalysis; metal ions will be dissolved in the aqueous solution, which causes difficult separation from solution. Therefore, the production cost is greatly increased due to its difficult recycling nature, and it is easy to cause secondary pollution to the environment. Therefore, $MeFe_2O_4$ with a low metal leaching rate has become a new research direction. Through PS/PMS [1] heterogeneous catalytic technology, these problems can be effectively solved [2][3][4].

At present, there are several common methods for preparing iron-based catalysts: hydrothermal, solvothermal, sol–gel preparation, and coprecipitation methods.

In the hydrothermal method, the solute is dispersed into the solution, stirred, and heated in the reactor, and finally washed and dried to obtain the required product [5].

Similar to the hydrothermal method, the solvothermal method changes water into an organic solvent. By dissolving one or more precursors in a nonaqueous solvent, the reaction occurs in liquid phase or supercritical conditions [6].

The sol–gel method is to dissolve the metal alkoxides in organic solvents, form homogeneous solutions, add other components, react at a certain temperature to form gels, and finally make products by drying [7].

Coprecipitation is an important method to prepare composite oxide ultrafine powder containing a large variety of metal elements [8].

The electron transfer between transition metal oxides is much higher [9] than that between single transition metal oxides. Generally, AB_2O_4 [10][11] structure is referred to as spinel structure. $CuFe_2O_4$ is a typical spinel ferrite with a magnetic structure, which has high chemical stability and low metal leaching rate. Taking $CuFe_2O_4$ as an example, compared with single transition metal oxides, Fe and Cu elements can play a role in the reaction; respectively, they can also activate PS to produce ·OH and $\cdot SO_4^-$.

G. Xian et al. [12] comprehensively compared the catalytic degradation effects of $CoFe_2O_4$, $CuFe_2O_4$, $MnFe_2O_4$, and $ZnFe_2O_4$. In detail, $CuFe_2O_4$ presented the best and fastest catalytic performance in organics removal. Almost 87.6% azo dye acid orange 7 (AO7) was removed in PS solution coupled with $CuFe_2O_4$ [12]. Additionally, it was known that

$CuFe_2O_4$ had the best catalytic effect. Moreover, through the quenching experiment, it was not ·OH but $\cdot SO_4^-$ that played a major role in the reaction.

Table 1 shows the degradation effects of some different $MeFe_2O_4$-activated PS/PMS on different kinds of wastewater. It can be seen from the table that the iron-based catalyst with spinel structure mainly acts on $\cdot SO_4^-$ in the mechanism of activation persulfate; the effect of ·OH is slightly worse [13]. Of course, there are also some nonfree radical pathways, which degrade pollutants in water by generating singlet oxygen $^1O_2$ [14][15][16].

Table 1. Effect of Different $MeFe_2O_4$-activated PMS on degradation of different wastewater [5][6][7][8][13][17][18][19].

Catalyst	Pollution	Main Mechanism	Pollutant Concentration	Catalyst Concentration	Oxidant	Oxidation Concentration	T/min	Degradation Rate/%	Number of Cycles	Synthesis Techniques	Ref.
$PbFe_2O_4$	Thionine	$^1O_2$	10 μM	0.4 g/L	PMS	400 μM	20	100	Not mentioned	Solution combustion	[17]
$CoFe_2O_4$–loaded quartz sand	Sulfachloropyridazine sodium	$\cdot SO_4^-$ ·OH	2 g/L	10 g	PMS	75 mg/L	150	90	Not mentioned	Citrate combustion	[18]
$CoFe_2O_4$-SAC	Norfloxacin (NOF)	$\cdot SO_4^-$ ·OH	10 mg/L	0.1 g/L	PMS	0.15 g/L	120	TOC reduction 81	5 (>80%)	Hydrothermal	[13]
The biochar loaded with $CoFe_2O_4$ nanoparticles	Bisphenol A (BPA)	$\cdot SO_4^-$ ·OH	10 mg/L	0.05 g/L	PMS	0.5 g/L	8	93	Not mentioned	Hydrothermal	[5]
C_3N_4@$MnFe_2O_4$-graphene	Metronidazole	$\cdot SO_4^-$ ·OH	20 mg/L	1.0 g/L	PS	0.01 M	90	94.5	5 (>80%)	Solvothermal	[6]
$Zn_{0.8}Cu_{0.2}Fe_2O_4$	Atrazine	$\cdot SO_4^-$	4.4 μM	200 mg/L	PS	0.5 mM	30	95	Not mentioned	Sol–gel	[7]
$CuFe_2O_4/O_3$	2,4-Dichlorophenoxyacetic acid (2,4-D)	Not mentioned	20 mg/L	0.20 g/L	PMS O_3	PMS 2.0 mM; O_3 16.0 mg/L;	40	88.9	5 (>80%)	Coprecipitation	[8]
$CoFe_2O_4$	Atrazine (ATZ)	$\cdot SO_4^-$	10 mg/L	0.4 g/L	PMS	0.8 mM	30	>99	5 (>60%)	Hydrothermal	[19]

2. $MeFe_2O_4$ Combined with the Carrier

The carrier recombination method can increase the specific surface area and increase the contact of chemical sites [20], thus greatly improving the rate of chemical reaction. At present, SiO_2 [20][21], black phosphorus [22][23], and rGO [24][25] (reduced graphene oxide) are commonly used as carriers. After compositing with the carrier, it is closely combined with the carrier by van der Waals force [24] or electrostatic interaction [26], making it difficult to fall off the surface of the carrier.

Pure graphene is a benzene-ring-like two-dimensional nanomaterial consisting of sp^2 hybrid orbitals. However, its high production cost limits its large-scale application. Afterward, by improving Hummer's method, a large number of oxygen-containing functional groups were linked at the edge of the plane by a strong oxidant, hence the name GO (graphene oxide) (**Figure 1**); rGO (**Figure 2**) was obtained by sodium borohydride and other means of reduction, which has low synthesis cost and is suitable for use as a good carrier of catalysis.

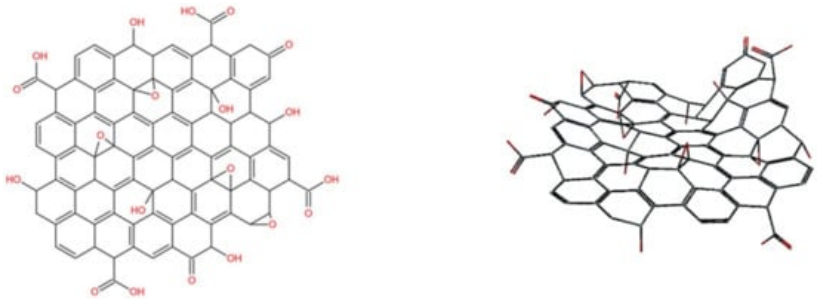

Figure 1. Plane structure (**left**) and solid structure (**right**) of GO (bond line type).

Figure 2. Plane structure (**left**) and solid structure (**right**) of rGO (bond line type).

Taking $CuFe_2O_4$, a representative of $MeFe_2O_4$, as an example, by comparing the effect of pure $CuFe_2O_4$ with that of $CuFe_2O_4$ combined with the carrier, it can be seen that the latter has a stronger catalytic effect under acidic and photoinduced conditions [27]. $CuFe_2O_4$ in $CuFe_2O_4$–rGO is closely combined with the oxygen-containing groups on rGO through electrostatic interaction, as shown in **Figure 3**. Images from a scanning electron microscope are shown in **Figure 4**.

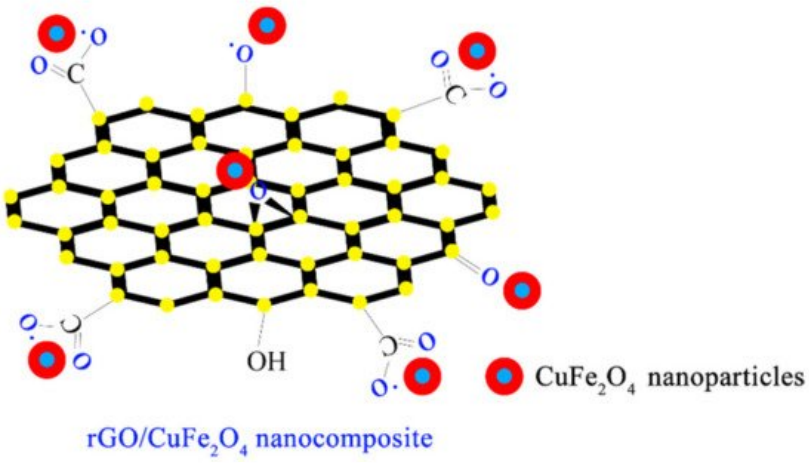

Figure 3. Chemical structural formula of $CuFe_2O_4$-rGO [26].

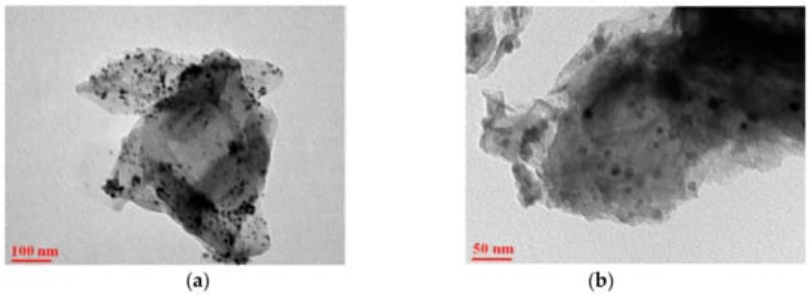

Figure 4. TEM images of (**a**,**b**) rGO/$CuFe_2O_4$ nanostructures under different magnifications [26].

Table 2 shows the degradation effects of some $CuFe_2O_4$ and rGO composite materials on different kinds of wastewater. It can be seen from the table that the composite catalyst can still produce good effects even without the presence of PS. Not only the Cu, Fe, and other elements in the catalyst can produce pure chemical catalytic effect, but the carrier rGO can produce electron transition under the light condition, promoting the transfer of electrons, and plays a part of the photocatalytic effect [28][29]. **Table 2** contains some other carriers, which can also greatly influence degradation of different kinds of wastewater.

Table 2. Effects of partial $MeFe_2O_4$ and carrier composite materials on degradation of different kinds of wastewater [27][30][31][32][33][34][35][36].

Catalyst	Pollution	Main Mechanism	Pollutant Concentration	Catalyst Concentration	Oxidant	Oxidation Concentration	T/min	Degradation Rate /%	Number of Cycles	Synthesis Techniques	Ref.
$CuFe_2O_4$-20%rGO	Methylparaben	SO_4^{-}··OH	10 mg/L	0.2 mg/L	PS	5 mM	120	96	Not mentioned	Sol-gel	[30]
$CuFe_2O_4$-1% (*w*/*w*) rGO	Phenol	·OH	20 ppm	5 mL	30% H_2O_2	6 mg/L	240	100	Not mentioned	Coprecipitation	[27]
$CuFe_2O_4$/g-C_3N_4	Propranolol	SO_4^{-}·	0.02 mM	1 g/L	PS	1 mM	120	82.2	Not mentioned	Sol-gel	[31]
$CoFe_2O_4$/CCNF	Dimethyl phthalate	SO_4^{-}·	0.05 mM	0.5 g/L	PMS	1.5 mM	60	>90	5 (>90%)	Sol-gel	[32]
TiO_2@$CuFe_2O_4$/UV	2,4-D	SO_4^{-}·	20 mg/L	0.1 g/L	PMS	0.3 mM	60	97.2	5 (>90%)	Sol-gel	[33]
ZnS-$ZnFe_2O_4$	Rhodamine B	SO_4^{-}·	20 mg/L	20 mg	PS	5 mg	90	97.67	3 (>95%)	Hydrothermal	[34]

Catalyst	Pollution	Main Mechanism	Pollutant Concentration	Catalyst Concentration	Oxidant	Oxidation Concentration	T/min	Degradation Rate /%	Number of Cycles	Synthesis Techniques	Ref.
Fe_2O_3@$CoFe_2O_4$	NOF	$SO_4^{\cdot-}$, ·OH	15 μM	0.3 g/L	PMS	0.4 mM	25	89.8	4 (90%)	Hydrothermal	[35]
Nitrogen and sulfur codoped C nanotube loaded $CuFe_2O_4$	2-Phenylbenzimidazole-5-sulfonic acid	$SO_4^{\cdot-}$, ·OH	5 mg/L	50 mg/L	PMS	1:100 (molar ratio)	40	98	5 (>85%)	Coprecipitation	[36]

3. Activation Persulfate by Fe^0

In recent years, activation persulfate based on Fe^0 (zero-valent iron, ZVI) have been widely used in chemical production and environmental remediation [34][38]. As mentioned above, the activation persulfate/Fe (II) mechanism can cause secondary pollution to water, so ZVI/PS [39][40] is used instead to reduce a series of problems caused by the reduction of Fe^{2+} content due to the change of pH and other factors in water [37].

ZVI/PS system has strong reducibility (Fe^0,E^0 = −0.44 V) [41]. Compared with $CuFe_2O_4$, its reaction process is more complex, as shown in **Figure 5**. Fe^0 is first converted to Fe^{2+} in the presence of acid and oxidant, then further oxidized to Fe^{3+} by Fe^{2+}, and finally to Fe(IV) [42][43]. The reaction mechanism follows [44]: According to the reaction equation, the reaction is easily affected by pH, and the reaction will gradually slow with the increase of pH. Weng et al. [45] point out that the Fe^0/PS system exhibits two-stage kinetics. The kinetic first stage is mostly attributed to a heterogeneous reaction occurring on the surface of the Fe^0 aggregate. As the reaction proceeds, decolorization shifts from the slow kinetic first stage to the fast kinetic second stage when sufficient Fe^{2+} ions are maintained in the system [46].

$$Fe^0 + 2H^+ \rightarrow Fe^{2+} + H_2$$

(2)

$$2Fe^0 + O_2 + 2H_2O \rightarrow 2Fe^{2+} + 4OH^-$$

(3)

$$Fe^0 + S_2O_8^{2-} \rightarrow Fe^{2+} + 2SO_4^{2-}$$

(4)

$$Fe^0 + HSO_5^- \rightarrow Fe^{2+} + SO_4^{2-} + OH^-$$

(5)

$$Fe^{2+} + S_2O_8^{2-} \rightarrow Fe^{3+} + SO_4^{2-} + \cdot SO_4^-$$

(6)

$$Fe^{2+} + HSO_5^- \rightarrow Fe^{3+} + SO_4^{2-} + \cdot SO_4^-$$

(7)

$$Fe^0 + S_2O_8^{2-} \rightarrow Fe^{2+} + 2\cdot SO_4^- + SO_4^{2-}$$

(8)

$$Fe^0 + 2\,HSO_5^- \rightarrow Fe^{2+} + 2OH^- + 2\cdot SO_4^-$$

(9)

$$Fe^{2+} + S_2O_8^{2-} + H_2O \rightarrow Fe^{IV}O^{2+} + 2SO_4^{2-} + 2H^+$$

(10)

$$Fe^{2+} + HSO_5^- \rightarrow Fe^{IV}O^{2+} + SO_4^{2-} + H^+$$

(11)

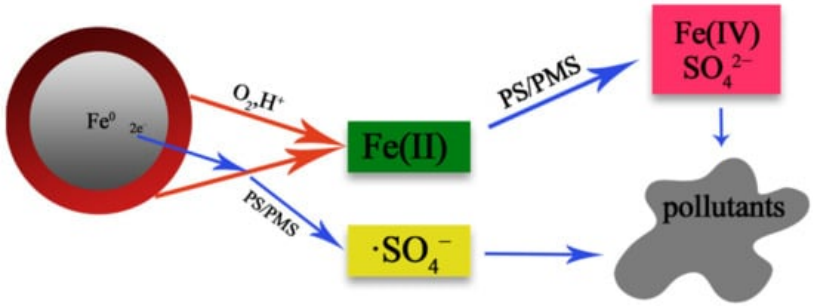

Figure 5. Schematic of the formation of $\cdot SO_4^-$ and Fe(IV) in nZVI/persulfate systems containing methyl phenyl sulfoxide [47].

Figure 6 shows the proposed degradation pathway of 2,4-D [48]. By examining **Figure 6**, it can further confirm that macromolecular organic matter is decomposed into small molecular organic matter, which is gradually mineralized.

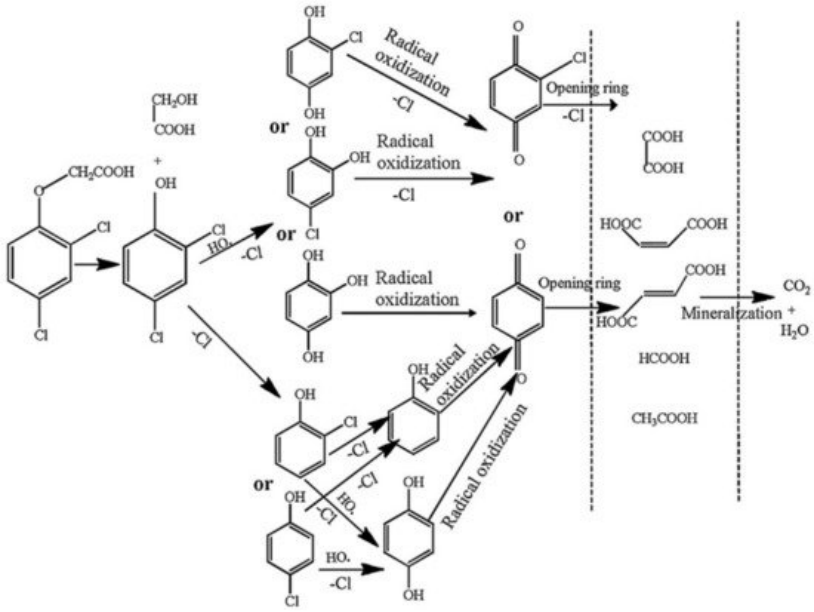

Figure 6. The proposed degradation pathway of 2,4-D [48].

Table 3 shows the degradation effects of various types of polluted water bodies activated by PS/PMS based on elemental iron. Usually, an appropriate amount of H_2O_2 [49] will be added to the water when PS is activated by Fe^0, so as to reduce the cost of oxidant. Through the analysis of the table, it can be seen that the effect of ZVI when used alone [50] is worse than when it is combined with the carrier or when other conditions exist.

Table 3. Degradation effect of different kinds of wastewater based on PS/PMS activated by different kinds of iron [51][52][53][54][55][56][57][58].

Catalyst	Pollution	Main Mechanism	Pollutant Concentration	Catalyst Concentration	Oxidant	Oxidation Concentration	T/min	Degradation Rate /%	Number of Cycles	Synthesis Techniques	Ref.
nZVI	Sulfamethazine	·OH $\cdot SO_4^-$	50 mg/L	2 mM	PS H_2O_2	1 mM 0.5 mM	30	96	Not mentioned	Sol-gel	[54]
CN-Fe	Sulfamethazine	$\cdot SO_4^-$ ·OH $^1O_2$	50 μM	0.5 g/L	PMS	1 mM	15	82	Not mentioned	Carbothermal	[53]
Carbon-coated nZVI	4-chlorophenol	$\cdot SO_4^-$ ·OH	150 μM	0.25 g/L	PMS	1 mM	120	96	Not mentioned	Commercially available	[52]
US-nZVI	Chloramphenicol	$\cdot SO_4^-$ ·OH	5 mg/L	0.5 g/L	PMS	1 mM	90	98.1	Not mentioned	Liquid phase reduction	[51]
$Fe^0@Fe_3O_4$	Dibutyl phthalate	·OH $\cdot SO_4^-$	18 μM	0.5 g L^{-1}	PS	1.8 mM	180	94.7	6 (>68%)	Calcination	[55]
$Fe^0@Fe_3O_4$	Atrazine	·OH $\cdot SO_4^-$	500 μg/L	25 mg/L	PMS	1 mM	2	100	Not mentioned	Reduction	[56]

Catalyst	Pollution	Main Mechanism	Pollutant Concentration	Catalyst Concentration	Oxidant	Oxidation Concentration	T/min	Degradation Rate /%	Number of Cycles	Synthesis Techniques	Ref.
Fe@C	Bisphenol S	·OH $\cdot SO_4^-$	5 mg/L	0.5 g/L	PMS	1.0 mM	60	92.8	Not mentioned	Resin carbonization	[57]
Fe@C/PB	2,4-Dichlorophenol	·OH $\cdot SO_4^-$	20 mg/L	0.6 g/L	PMS	2.0 g/L	50	99.4	Not mentioned	Calcination	[58]

4. Fe_3O_4

Fe_3O_4 magnetite, also known as magnetic iron oxide, is a black crystal with a rotating spinel structure (**Figure 7**). In magnetite, Fe^{2+} and Fe^{3+} are disordered on the ferrite octahedron, so electrons can transfer rapidly between Fe^{2+} and Fe^{3+}; thus, reversible redox reactions can occur at the same position on the octahedron.

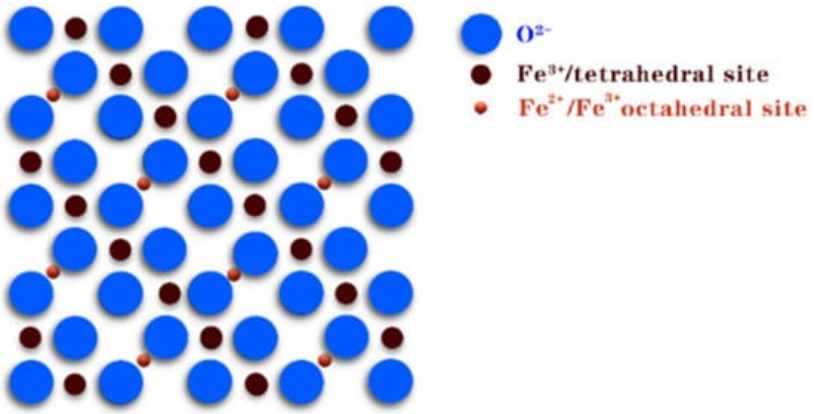

Figure 7. Crystal structure of Fe_3O_4.

However, since Fe_3O_4 is easy to accumulate in solution and contact sites are reduced after agglomeration, single Fe_3O_4 is rarely used. Using the composite carrier method [59] can not only solve these problems, but also speeds the reaction rate, making it more cost effective when applied in industrial production. He et al. [60] pointed out that the Fe_3O_4/GO/Ag composite microspheres are formed using magnetic Fe_3O_4 as cores, followed by coating an internal layer of GO and an outer layer of Ag nanoparticles, as **Figure 8** shows. The synthesized Fe_3O_4/GO/Ag composite catalyst under the action of $NaBH_4$, methylene blue, and ciprofloxacin can be completely degraded within 12 min. **Figure 8** shows SEM images of Fe_3O_4/GO/Ag composite catalyst. In **Figure 9**, we can clearly observe that Ag has been completely attached to the Fe_3O_4/GO surface, which can increase the specific surface area and improve the chemical reaction rate.

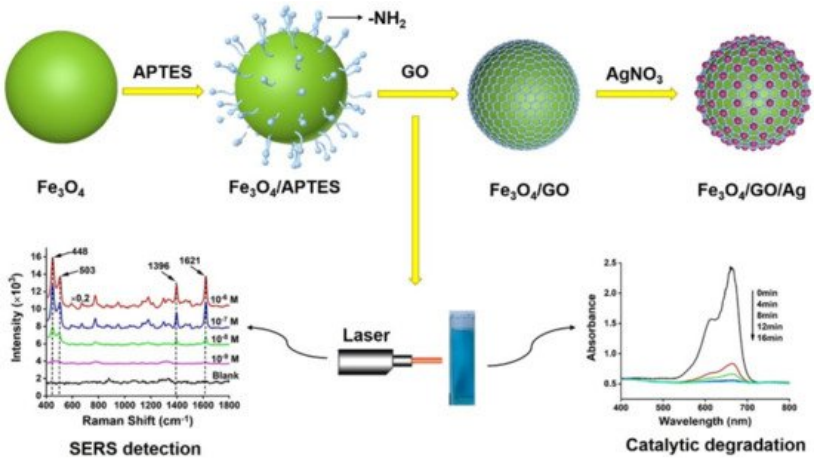

Figure 8. Illustration of the fabrication of Fe_3O_4/GO/Ag composite microspheres [60].

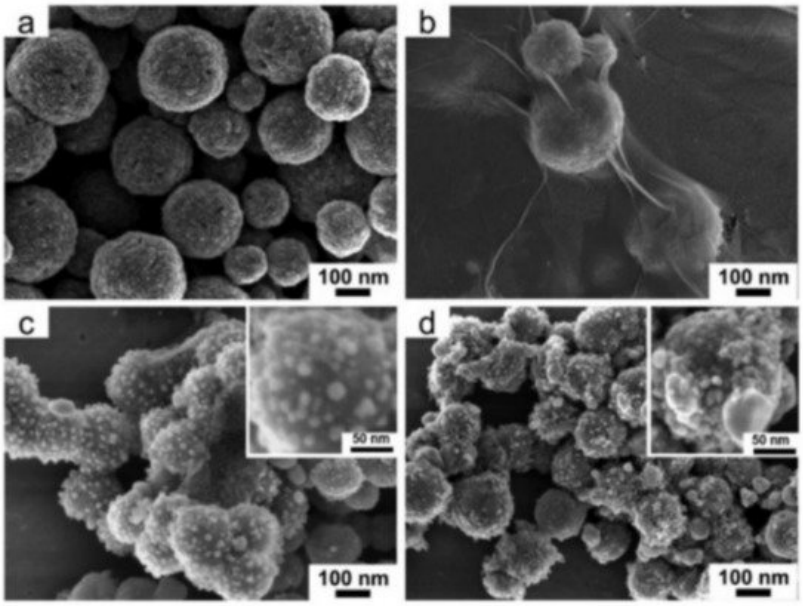

Figure 9. Typical FESEM images of (**a**) Fe_3O_4, (**b**) Fe_3O_4/GO, (**c**) Fe_3O_4/GO/Ag, and (**d**) Fe_3O_4/Ag microspheres. Inserts are magnified FESEM images of Fe_3O_4/GO/Ag and Fe_3O_4/Ag microspheres [60].

Table 4 shows the research progress of Fe_3O_4 and its composite materials on the degradation of different pollutants reported at present. According to the data in the table, when Fe_3O_4 is compounded with the carrier, the catalytic performance is greatly improved.

Table 4. Effects of Fe_3O_4 and its composite-material-activated PS/PMS on degradation of different kinds of wastewater [61][62][63][64][65][66][67].

Catalyst	Pollution	Main Mechanism	Pollutant Concentration	Catalyst Concentration	Oxidant	Oxidation Concentration	T/min	Degradation Rate /%	Number of Cycles	Synthesis Techniques	Ref.
Fe_3O_4	BPA	$\cdot SO_4^-$ $\cdot OH$	20 mg/L	2.0 g/L	PMS	5 mM	30	27.53	Not mentioned	Commercially available	[61]
CuO-Fe_3O_4-BC	BPA	$\cdot SO_4^-$ $\cdot OH$	20 mg/L	2.0 g/L	PMS	5 mM	30	100	4 (>85%)	Coprecipitation	[62]
rGO-Fe_3O_4	NOF	$^1O_2$ $\cdot OH$ $\cdot SO_4^-$	20 mg/L	0.5 g/L	PS	1 g/L	30	89.69	Not mentioned	Coprecipitation	[62]
Fe_3O_4	Sulfamonomethoxine	$\cdot SO_4^-$	0.06 mM	2.4 mM	PS	1.2 mM	15	100	Not mentioned	Coprecipitation	[63]
Fe_3O_4@Zn/Co-ZIFs	Carbamazepine	$\cdot SO_4^-$	5 mg/L	25 mg/L	PMS	0.4 mM	30	100	Not mentioned	Solvothermal	[64]
Fe_3O_4/microwave irradiation (3 kW/L)	p-Nitrophenol	$\cdot SO_4^-$	20 mg/L	2.5 g/L	PS	15:1 (molar ratio)	28	94.2	Not mentioned	Not mentioned	[65]
Fe_3O_4/MC	p-Hydroxybenzoic acid	$\cdot SO_4^-$	1.0 g/L	0.2 g/L	PS	1.0 g/L	30	100	Not mentioned	Sol-gel	[66]
Fe_3O_4/graphene aerogels	Malachite green	Not mentioned	20 mg/L	0.2 g/L	PS	1.0 mM	12	91.7	Not mentioned	Sol-gel	[67]

@: the composite of two materials.

References

1. Fan, X.; Wang, Y.; Zhang, D.; Guo, Y.; Gao, S.; Li, E.; Zheng, H. Effects of acid, acid-ZVI/PMS, Fe(II)/PMS and ZVI/PMS conditioning on the wastewater activated sludge (WAS) dewaterability and extracellular polymeric substances (EPS). J. Environ. Sci. 2020, 91, 73–84.
2. Li, Y.; Zhu, W.; Guo, Q.; Wang, X.; Zhang, L.; Gao, X.; Luo, Y. Highly efficient degradation of sulfamethoxazole (SMX) by activating peroxymonosulfate (PMS) with CoFe2O4 in a wide pH range. Sep. Purif. Technol. 2021, 276, 119403.
3. Wei, W.; Zhou, D.; Feng, L.; Li, X.; Hu, L.; Zheng, H.; Wang, Y. The graceful art, significant function and wide application behavior of ultrasound research and understanding in carbamazepine (CBZ) enhanced removal and degradation by Fe0/PDS/US. Chemosphere 2021, 278, 130368.
4. Wang, J.; Wang, S. Activation of persulfate (PS) and peroxymonosulfate (PMS) and application for the degradation of emerging contaminants. Chem. Eng. J. 2018, 334, 1502–1517.
5. Li, Y.; Ma, S.; Xu, S.; Fu, H.; Li, Z.; Li, K.; Sheng, K.; Du, J.; Lu, X.; Li, X.; et al. Novel magnetic biochar as an activator for peroxymonosulfate to degrade bisphenol A: Emphasizing the synergistic effect between graphitized structure and

CoFe2O4. Chem. Eng. J. 2020, 387, 124094.

6. Wang, X.; Wang, A.; Ma, J. Visible-light-driven photocatalytic removal of antibiotics by newly designed C3N4@MnFe2O4-graphene nanocomposites. J. Hazard. Mater. 2017, 336, 81–92.
7. Huang, Y.; Han, C.; Liu, Y.; Nadagouda, M.N.; Machala, L.; O'Shea, K.E.; Sharma, V.K.; Dionysiou, D.D. Degradation of atrazine by ZnxCu1−xFe2O4 nanomaterial-catalyzed sulfite under UV–vis light irradiation: Green strategy to generate SO4−. Appl. Catal. B Environ. 2018, 221, 380–392.
8. Jaafarzadeh, N.; Ghanbari, F.; Ahmadi, M. Efficient degradation of 2,4-dichlorophenoxyacetic acid by peroxymonosulfate/magnetic copper ferrite nanoparticles/ozone: A novel combination of advanced oxidation processes. Chem. Eng. J. 2017, 320, 436–447.
9. Song, Y.; Yang, Y.; Mo, S.; Guo, D.; Liu, L. Fast construction of (Fe2O3) heterostructure nanosheets as highly active catalyst for water oxidation. J. Alloys Compd. 2022, 892, 162149.
10. Lyu, L.; Won Kim, C.; Seong, K.-D.; Kang, J.; Liu, S.; Yamauchi, Y.; Piao, Y. Defect engineering induced heterostructure of ZnMn2O4 nanocrystal for flexible asymmetric supercapacitor. Chem. Eng. J. 2021, 133115.
11. Xie, X.; Wang, B.; Wang, Y.; Ni, C.; Sun, X.; Du, W. Spinel structured MFe2O4 (M = Fe, Co, Ni, Mn, Zn) and their composites for microwave absorption: A review. Chem. Eng. J. 2022, 428, 131160.
12. Xian, G.; Kong, S.; Li, Q.; Zhang, G.; Zhou, N.; Du, H.; Niu, L. Synthesis of Spinel Ferrite MFe2O4 (M = Co, Cu, Mn, and Zn) for Persulfate Activation to Remove Aqueous Organics: Effects of M-Site Metal and Synthetic Method. Front. Chem. 2020, 8.
13. Yang, Z.; Li, Y.; Zhang, X.; Cui, X.; He, S.; Liang, H.; Ding, A. Sludge activated carbon-based CoFe2O4-SAC nanocomposites used as heterogeneous catalysts for degrading antibiotic norfloxacin through activating peroxymonosulfate. Chem. Eng. J. 2020, 384, 123319.
14. Mostafa, S.; Rosario-Ortiz, F.L. Singlet oxygen formation from wastewater organic matter. Environ. Sci. Technol. 2013, 47, 8179–8186.
15. Yi, Q.; Ji, J.; Shen, B.; Dong, C.; Liu, J.; Zhang, J.; Xing, M. Singlet Oxygen Triggered by Superoxide Radicals in a Molybdenum Cocatalytic Fenton Reaction with Enhanced REDOX Activity in the Environment. Environ. Sci. Technol. 2019, 53, 9725–9733.
16. Mikrut, M.; Mazuryk, O.; Macyk, W.; van Eldik, R.; Stochel, G. Generation and photogeneration of hydroxyl radicals and singlet oxygen by particulate matter and its inorganic components. J. Environ. Chem. Eng. 2021, 9, 106478.
17. Liu, F.; Li, W.; Wu, D.; Tian, T.; Wu, J.-F.; Dong, Z.-M.; Zhao, G.-C. New insight into the mechanism of peroxymonosulfate activation by nanoscaled lead-based spinel for organic matters degradation: A singlet oxygen-dominated oxidation process. J. Colloid Interface Sci. 2020, 572, 318–327.
18. Gao, D.; Junaid, M.; Lin, F.; Zhang, S.; Xu, N. Degradation of sulphachloropyridazine sodium in column reactor packed with CoFe2O4−loaded quartz sand via peroxymonosulfate activation: Insights into the amorphous phase, efficiency, and mechanism. Chem. Eng. J. 2020, 390, 124549.
19. Li, J.; Xu, M.; Yao, G.; Lai, B. Enhancement of the degradation of atrazine through CoFe2O4 activated peroxymonosulfate (PMS) process: Kinetic, degradation intermediates, and toxicity evaluation. Chem. Eng. J. 2018, 348, 1012–1024.
20. Ratanaphain, C.; Viboonratanasri, D.; Prompinit, P.; Krajangpan, S.; Khan, E.; Punyapalakul, P. Reactivity characterization of SiO2-coated nano zero-valent iron for iodoacetamide degradation: The effects of SiO2 thickness, and the roles of dehalogenation, hydrolysis and adsorption. Chemosphere 2022, 286, 131816.
21. Ding, S.; Wan, J.; Wang, Y.; Yan, Z.; Ma, Y. Activation of persulfate by molecularly imprinted 2 for the targeted degradation of dimethyl phthalate: Effects of operating parameters and chlorine. Chem. Eng. J. 2021, 422, 130406.
22. Wang, L.; Guan, R.; Qi, Y.; Zhang, F.; Li, P.; Wang, J.; Qu, P.; Zhou, G.; Shi, W. Constructing Zn-P charge transfer bridge over ZnFe2O4-black phosphorus 3D microcavity structure: Efficient photocatalyst design in visible-near-infrared region. J. Colloid Interface Sci. 2021, 600, 463–472.
23. Shao, S.; Deng, J.; Lv, X.; Ji, H.; Xiao, Y.; Zhu, X.; Feng, K.; Xu, H.; Zhong, J. Black phosphorus nanoflakes decorated hematite photoanode with functional phosphate bridges for enhanced water oxidation. Chem. Eng. J. 2021, 425, 131500.
24. Askari, M.B.; Salarizadeh, P.; Beitollahi, H.; Tajik, S.; Eshghi, A.; Azizi, S. Electro-oxidation of hydrazine on NiFe2O4-rGO as a high-performance nano-electrocatalyst in alkaline media. Mater. Chem. Phys. 2022, 275, 125313.
25. Wang, X.; Wang, D.; Ma, C.; Yang, Z.; Yue, H.; Zhang, D.; Sun, Z. Conductive Fe2N/N-rGO composite boosts electrochemical redox reactions in wide temperature accommodating lithium-sulfur batteries. Chem. Eng. J. 2022, 427,

131622.

26. Karthikeyan, C.; Ramachandran, K.; Sheet, S.; Yoo, D.J.; Lee, Y.S.; Satish kumar, Y.; Kim, A.R.; Gnana kumar, G. Pigeon-Excreta-Mediated Synthesis of Reduced Graphene Oxide (rGO)/CuFe2O4 Nanocomposite and Its Catalytic Activity toward Sensitive and Selective Hydrogen Peroxide Detection. ACS Sustain. Chem. Eng. 2017, 5, 4897–4905.
27. Othman, I.; Abu Haija, M.; Ismail, I.; Zain, J.H.; Banat, F. Preparation and catalytic performance of CuFe2O4 nanoparticles supported on reduced graphene oxide (CuFe2O4/rGO) for phenol degradation. Mater. Chem. Phys. 2019, 238.
28. Wang, W.; Yu, J.C.; Xia, D.; Wong, P.K.; Li, Y. Graphene and g-C3N4 nanosheets cowrapped elemental alpha-sulfur as a novel metal-free heterojunction photocatalyst for bacterial inactivation under visible-light. Environ. Sci. Technol. 2013, 47, 8724–8732.
29. Sun, B.; Ma, W.; Wang, N.; Xu, P.; Zhang, L.; Wang, B.; Zhao, H.; Lin, K.A.; Du, Y. Retraction of “Polyaniline: A New Metal-Free Catalyst for Peroxymonosulfate Activation with Highly Efficient and Durable Removal of Organic Pollutants”. Environ. Sci. Technol. 2021, 55, 3451.
30. Hao, P.; Hu, M.; Xing, R.; Zhou, W. Synergistic degradation of methylparaben on CuFe2O4-rGO composite by persulfate activation. J. Alloys Compd. 2020, 823, 153757.
31. Li, R.; Cai, M.; Xie, Z.; Zhang, Q.; Zeng, Y.; Liu, H.; Liu, G.; Lv, W. Construction of heterostructured CuFe2O4/g-C3N4 nanocomposite as an efficient visible light photocatalyst with peroxydisulfate for the organic oxidation. Appl. Catal. B Environ. 2019, 244, 974–982.
32. Gan, L.; Zhong, Q.; Geng, A.; Wang, L.; Song, C.; Han, S.; Cui, J.; Xu, L. Cellulose derived carbon nanofiber: A promising biochar support to enhance the catalytic performance of CoFe2O4 in activating peroxymonosulfate for recycled dimethyl phthalate degradation. Sci. Total Environ. 2019, 694, 133705.
33. Golshan, M.; Kakavandi, B.; Ahmadi, M.; Azizi, M. Photocatalytic activation of peroxymonosulfate by TiO2 anchored on cupper ferrite (TiO2@CuFe2O4) into 2,4-D degradation: Process feasibility, mechanism and pathway. J. Hazard. Mater. 2018, 359, 325–337.
34. Zhu, B.; Cheng, H.; Ma, J.; Kong, Y.; Komarneni, S. Efficient degradation of rhodamine B by magnetically separable ZnS–ZnFe2O4 composite with the synergistic effect from persulfate. Chemosphere 2019, 237, 124547.
35. Kohantorabi, M.; Hosseinifard, M.; Kazemzadeh, A. Catalytic activity of a magnetic Fe2O3@CoFe2O4 nanocomposite in peroxymonosulfate activation for norfloxacin removal. N. J. Chem. 2020, 44, 4185–4198.
36. Zhang, X.; Feng, M.; Wang, L.; Qu, R.; Wang, Z. Catalytic degradation of 2-phenylbenzimidazole-5-sulfonic acid by peroxymonosulfate activated with nitrogen and sulfur co-doped CNTs-COOH loaded CuFe2O4. Chem. Eng. J. 2017, 307, 95–104.
37. Cuervo Lumbaque, E.; Lopes Tiburtius, E.R.; Barreto-Rodrigues, M.; Sirtori, C. Current trends in the use of zero-valent iron (Fe0) for degradation of pharmaceuticals present in different water matrices. Trends Environ. Anal. Chem. 2019, 24, e00069.
38. Hussain, I.; Zhang, Y.; Huang, S.; Gao, Q. Degradation of p-chloroaniline by FeO3−xH3−2x/Fe0 in the presence of persulfate in aqueous solution. RSC Adv. 2015, 5, 41079–41087.
39. Rodriguez, S.; Vasquez, L.; Romero, A.; Santos, A. Dye Oxidation in Aqueous Phase by Using Zero-Valent Iron as Persulfate Activator: Kinetic Model and Effect of Particle Size. Ind. Eng. Chem. Res. 2014, 53, 12288–12294.
40. Li, J.; Zhang, X.; Sun, Y.; Liang, L.; Pan, B.; Zhang, W.; Guan, X. Advances in Sulfidation of Zerovalent Iron for Water Decontamination. Environ. Sci. Technol. 2017, 51, 13533–13544.
41. Xiao, S.; Cheng, M.; Zhong, H.; Liu, Z.; Liu, Y.; Yang, X.; Liang, Q. Iron-mediated activation of persulfate and peroxymonosulfate in both homogeneous and heterogeneous ways: A review. Chem. Eng. J. 2020, 384, 123265.
42. Wang, Z.; Qiu, W.; Pang, S.-Y.; Zhou, Y.; Gao, Y.; Guan, C.; Jiang, J. Further understanding the involvement of Fe(IV) in peroxydisulfate and peroxymonosulfate activation by Fe(II) for oxidative water treatment. Chem. Eng. J. 2019, 371, 842–847.
43. Huang, J.; Zhang, H. Mn-based catalysts for sulfate radical-based advanced oxidation processes: A review. Environ. Int. 2019, 133, 105141.
44. Zheng, X.; Niu, X.; Zhang, D.; Lv, M.; Ye, X.; Ma, J.; Lin, Z.; Fu, M. Metal-based catalysts for persulfate and peroxymonosulfate activation in heterogeneous ways: A review. Chem. Eng. J. 2022, 429, 132323.
45. Weng, C.H.; Ding, F.; Lin, Y.T.; Liu, N. Effective decolorization of polyazo direct dye Sirius Red F3B using persulfate activated with Fe-0 aggregate. Sep. Purif. Technol. 2015, 147, 147–155.

46. Li, H.; Wan, J.; Ma, Y.; Wang, Y.; Huang, M. Influence of particle size of zero-valent iron and dissolved silica on the reactivity of activated persulfate for degradation of acid orange 7. Chem. Eng. J. 2014, 237, 487–496.

47. Wang, Z.; Qiu, W.; Pang, S.; Gao, Y.; Zhou, Y.; Cao, Y.; Jiang, J. Relative contribution of ferryl ion species (Fe(IV)) and sulfate radical formed in nanoscale zero valent iron activated peroxydisulfate and peroxymonosulfate processes. Water Res. 2020, 172, 115504.

48. Li, X.; Zhou, M.; Pan, Y. Enhanced degradation of 2,4-dichlorophenoxyacetic acid by pre-magnetization Fe-C activated persulfate: Influential factors, mechanism and degradation pathway. J. Hazard. Mater. 2018, 353, 454–465.

49. Ye, C.; Liu, P.; Ma, Z.; Xue, C.; Zhang, C.; Zhang, Y.; Liu, J.; Liu, C.; Sun, X.; Mu, Y. High H2O2 Concentrations Observed during Haze Periods during the Winter in Beijing: Importance of H2O2 Oxidation in Sulfate Formation. Environ. Sci. Technol. Lett. 2018, 5, 757–763.

50. Peng, X.; Xi, B.; Zhao, Y.; Shi, Q.; Meng, X.; Mao, X.; Jiang, Y.; Ma, Z.; Tan, W.; Liu, H.; et al. Effect of Arsenic on the Formation and Adsorption Property of Ferric Hydroxide Precipitates in ZVI Treatment. Environ. Sci. Technol. 2017, 51, 10100–10108.

51. Wu, J.; Wang, B.; Cagnetta, G.; Huang, J.; Wang, Y.; Deng, S.; Yu, G. Nanoscale zero valent iron-activated persulfate coupled with Fenton oxidation process for typical pharmaceuticals and personal care products degradation. Sep. Purif. Technol. 2020, 239, 116534.

52. Zhang, T.; Yang, Y.; Gao, J.; Li, X.; Yu, H.; Wang, N.; Du, P.; Yu, R.; Li, H.; Fan, X.; et al. Synergistic degradation of chloramphenicol by ultrasound-enhanced nanoscale zero-valent iron/persulfate treatment. Sep. Purif. Technol. 2020, 240, 116575.

53. Chen, L.; Huang, Y.; Zhou, M.; Xing, K.; Lv, W.; Wang, W.; Chen, H.; Yao, Y. Nitrogen-doped porous carbon encapsulating iron nanoparticles for enhanced sulfathiazole removal via peroxymonosulfate activation. Chemosphere 2020, 250, 126300.

54. Li, S.; Tang, J.; Liu, Q.; Liu, X.; Gao, B. A novel stabilized carbon-coated nZVI as heterogeneous persulfate catalyst for enhanced degradation of 4-chlorophenol. Environ. Int. 2020, 138, 105639.

55. Li, H.; Wan, J.; Ma, Y.; Wang, Y. Synthesis of novel core–shell Fe0@Fe3O4 as heterogeneous activator of persulfate for oxidation of dibutyl phthalate under neutral conditions. Chem. Eng. J. 2016, 301, 315–324.

56. Feng, Y.; Zhong, J.; Zhang, L.; Fan, Y.; Yang, Z.; Shih, K.; Li, H.; Wu, D.; Yan, B. Activation of peroxymonosulfate by Fe0@Fe3O4 core-shell nanowires for sulfate radical generation: Electron transfer and transformation products. Sep. Purif. Technol. 2020, 247, 116942.

57. Liu, Y.; Guo, H.; Zhang, Y.; Cheng, X.; Zhou, P.; Wang, J.; Li, W. carbonized resin for peroxymonosulfate activation and bisphenol S degradation. Environ. Pollut. 2019, 252, 1042–1050.

58. Guo, F.; Wang, K.; Lu, J.; Chen, J.; Dong, X.; Xia, D.; Zhang, A.; Wang, Q. Activation of peroxymonosulfate by magnetic carbon supported Prussian blue nanocomposite for the degradation of organic contaminants with singlet oxygen and superoxide radicals. Chemosphere 2019, 218, 1071–1081.

59. Wang, H.; Zhang, C.; Zhang, X.; Wang, S.; Xia, Z.; Zeng, G.; Ding, J.; Ren, N. Construction of Fe3O4@β-CD/g-C3N4 nanocomposite catalyst for degradation of PCBs in wastewater through photodegradation and heterogeneous Fenton oxidation. Chem. Eng. J. 2022, 429, 132445.

60. He, J.; Song, G.; Wang, X.; Zhou, L.; Li, J. Multifunctional magnetic Fe3O4/GO/Ag composite microspheres for SERS detection and catalytic degradation of methylene blue and ciprofloxacin. J. Alloys Compd. 2022, 893, 162226.

61. Zhen, J.; Zhang, S.; Zhuang, X.; Ahmad, S.; Lee, T.; Si, H.; Cao, C.; Ni, S.-Q. Sulfate radicals based heterogeneous peroxymonosulfate system catalyzed by CuO-Fe3O4-Biochar nanocomposite for bisphenol A degradation. J. Water Process Eng. 2021, 41, 102078.

62. Yin, F.; Wang, C.; Lin, K.-Y.A.; Tong, S. Persulfate activation for efficient degradation of norfloxacin by a rGO-Fe3O4 composite. J. Taiwan Inst. Chem. Eng. 2019, 102, 163–169.

63. Yan, J.; Lei, M.; Zhu, L.; Anjum, M.N.; Zou, J.; Tang, H. Degradation of sulfamonomethoxine with Fe3O4 magnetic nanoparticles as heterogeneous activator of persulfate. J. Hazard. Mater. 2011, 186, 1398–1404.

64. Wu, Z.; Wang, Y.; Xiong, Z.; Ao, Z.; Pu, S.; Yao, G.; Lai, B. Core-shell magnetic Fe3O4@Zn/Co-ZIFs to activate peroxymonosulfate for highly efficient degradation of carbamazepine. Appl. Catal. B Environ. 2020, 277, 119136.

65. Zhao, G.; Zou, J.; Chen, X.; Liu, L.; Wang, Y.; Zhou, S.; Long, X.; Yu, J.; Jiao, F. Iron-based catalysts for persulfate-based advanced oxidation process: Microstructure, property and tailoring. Chem. Eng. J. 2021, 421, 127845.

66. Fu, H.; Zhao, P.; Xu, S.; Cheng, G.; Li, Z.; Li, Y.; Li, K.; Ma, S. Fabrication of Fe3O4 and graphitized porous biochar composites for activating peroxymonosulfate to degrade p-hydroxybenzoic acid: Insights on the mechanism. Chem.

Eng. J. 2019, 375, 121980.

67. Lu, J.-D. The effect of two ferromagnetic metal stripes on valley polarization of electrons in a graphene. Phys. Lett. A 2020, 384, 126402.
